epl A Letters Journal Exploring the Frontiers of Physics

January 2018

EPL, **121** (2018) 14002 www.epljournal.org
doi: 10.1209/0295-5075/121/14002

Inertial floaters in stratified turbulence

A. Sozza, F. De Lillo and G. Boffetta

Department of Physics, Università di Torino & INFN - via P. Giuria 1, 10125 Torino, Italy

received 6 December 2017; accepted in final form 22 February 2018
published online 9 March 2018

PACS 47.27.T- – Turbulent transport processes
PACS 47.55.Hd – Stratified flows

Abstract – We investigate numerically the dynamics and statistics of inertial particles transported by stratified turbulence, in the case of particle density intermediate in the average density profile of the fluid. Under these conditions, particles tend to form a thin layer around the corresponding fluid isopycnal. The thickness of the resulting layer is determined by a balance between buoyancy (which attracts the particle to the isopycnal) and inertia (which prevents them from following it exactly). By means of extensive numerical simulations, we explore the parameter space of the system and we find that in a range of parameters particles form fractal clusters within the layer.

Introduction. – The interaction between particle inertia and turbulence is a fundamental issue for many problems in natural sciences and in applications, from cloud formation in the atmosphere to the dynamics of plankton in the ocean [1,2]. Most of the studies have considered the simplified case of inertial particles in homogeneous-isotropic turbulence [3–5], while more recent works have investigated the interaction between gravity and turbulent acceleration [6,7].

In the case of stratified turbulence, gravity plays two different roles: on the one hand it produces a vertical motion of inertial particles with respect to the flow which can increase sedimentation; on the other hand it generates a layered structure in the flow by reducing the vertical velocity fluctuations and promoting bidimensionalization [8,9].

The motion of inertial particles in stratified turbulence has been recently addressed by means of direct numerical simulations within the Boussinesq approximation of incompressible flow [10–12]. In particular, it has been shown that inertial particles clusterize for a wide range of parameters in a simplified overdamped limit in which inertia is felt only through the effect of gravity. In that limit, it has been found that vertical confinement due to density stratification induces a dissipative dynamics of the particles and this produces a strong fractal clustering on the isopycnal surface. Fractal clustering depends on a single parameter, combination of the Stokes time τ_p of the particles and the Brunt-Väisälä frequency of the flow. In the limit of small τ_p (*i.e.*, small inertia), in which that model is valid, clustering monotonically increases with τ_p [12].

In this letter we extend the previous investigation by considering the Maxey-Riley model for small inertial particles with finite inertia [13], similar to the model used in [10]. We confirm the vertical confinement of the particles induced by stratification and we explain the non-monotonic dependence on the parameters by introducing a simple stochastic model for the vertical motion. Small-scale fractal clustering, quantified by the fractal dimension of particle distribution, also displays a non-monotonic behavior, typical of inertial particles in incompressible flows, but with a peculiar scaling law for small Stokes numbers due to the presence of density stratification.

In this paper we will study the behavior of a widely used model for inertial particles [13] in order to go beyond the limit of small inertia in the description of layer formation. First, we will describe the numerical model for the flow and the particles and introduce the physical parameters controlling the dynamics. Then, we will present the numerical results on the vertical distribution of the floaters and the small-scale inhomogeneity. Finally, the results will be discussed in the conclusions.

Equation of motion for a floater. – We consider a fluid linearly and stably stratified in the gravity direction $\mathbf{g} = (0, 0, -g)$ with density profile $\rho = \rho_0 - \gamma(z-\theta)$. Within the Boussinesq approximation the equations of motion for the incompressible velocity $\mathbf{u}$ (with $\nabla \cdot \mathbf{u} = 0$) and the density fluctuation θ are

$$\partial_t \mathbf{u} + \mathbf{u} \cdot \nabla \mathbf{u} = -\nabla p - N^2 \theta \, \hat{\mathbf{z}} + \nu \nabla^2 \mathbf{u} + \mathbf{f}, \quad (1)$$

$$\partial_t \theta + \mathbf{u} \cdot \nabla \theta = w + \kappa \nabla^2 \theta, \quad (2)$$

where ν is the kinematic viscosity, κ is the diffusivity and $N^2 = \gamma g/\rho_0$ is the Brunt-Väisälä frequency. On the r.h.s., $\mathbf{f}$ represents an external forcing, which injects

energy in the system at a rate ε to maintain a stationary state, and is confined on a characteristic large-scale ℓ_f. For simplicity and numerical convenience we only consider the case with Prandtl number $Pr = \nu/\kappa = 1$. Three dimensionless parameters can be defined in terms of the viscous scale $\eta = (\nu^3/\epsilon)^{1/4}$, the Ozmidov scale $\ell_0 = (\epsilon/N^3)^{1/2}$ and the forcing scale ℓ_f: the Reynolds number $Re = (\ell_f/\eta)^{4/3}$, the Froude Number $Fr = \varepsilon^{1/3}\ell_f^{2/3}/N = (\ell_0/\ell_f)^{2/3}$ and the buoyancy Reynolds number $Re_b = Fr^2 Re = (\ell_0/\eta)^{4/3}$ [9].

Particles are assumed to be spherical with a density equal to the reference density ρ_0 of the fluid. This assumption simplifies the notation without loss of generality, since the flow is homogeneous. We also assume that their radius a and their velocity relative to the fluid, $\mathbf{v} - \mathbf{u}$, are small enough to guarantee creeping flow conditions around the particle, *i.e.*, with the particle's Reynolds number $Re_p = |\mathbf{v} - \mathbf{u}|a/\nu \ll 1$. Consistently with these assumptions, particle position $\mathbf{x}$ and velocity $\mathbf{v}$ are governed by a simplified version of the Maxey-Riley equation for spherical inertial particles [13], as

$$\dot{\mathbf{x}} = \mathbf{v}, \tag{3}$$

$$\dot{\mathbf{v}} = \beta \frac{D\mathbf{u}}{Dt} - \frac{\mathbf{v} - \mathbf{u}}{\tau_p} + (1 - \beta)\,\mathbf{g}. \tag{4}$$

The added mass term in eq. (4) is proportional to the time derivative along fluid trajectories (denoted by the material derivative D/Dt) of the fluid velocity $\mathbf{u}(\mathbf{x}, t)$ at the position of the particle. The parameter $\beta = 3\rho/(\rho + 2\rho_0)$ is a function of the ratio between the particle's density ρ_0 and the local density ρ of the surrounding fluid, while $\tau_p = a^2/(3\nu\beta)$ is the Stokes time. We remark that in eq. (4) we neglect the so-called Faxen's correction and the Basset's history term since they give a negligible contribution for small particles. Taking into account the expression for the density profile, we can write $(1-\beta)g \simeq \frac{2}{3}N^2(z-\theta)$. Except from the latter term, where density fluctuations survive because they are multiplied by the acceleration of gravity, the assumption $\beta \simeq 1$ can be safely made everywhere else in eq. (4). This reasoning is consistent with the Boussinesq approximation leading to eqs. (1), (2). One thus obtains

$$\dot{\mathbf{v}} = \frac{D\mathbf{u}}{Dt} - \frac{\mathbf{v} - \mathbf{u}}{\tau_p} - \frac{2}{3}N^2(z - \theta)\hat{\mathbf{z}}. \tag{5}$$

The dimensionless parameter which measures the particle inertia is the Stokes number $St = \tau_p/\tau_\eta$, where τ_η is the Kolmogorov time scale of the flow.

Numerical simulation. – We have performed direct numerical simulations of the Boussinesq equation for a stratified flow, eqs. (1), (2), in a periodic box of size $L = 2\pi$ by using a fully dealiased pseudo-spectral method in space with a second-order Runge-Kutta scheme for time evolution. Turbulence is maintained in a statistical steady state by a random δ-correlated in time forcing acting at large-scale in a narrow band of wave numbers peaked at $k_f \simeq 1/\ell_f$. We have used different spatial resolutions $M = 128, 256$, corresponding to Reynolds numbers $Re = (k_f\eta)^{-4/3} \sim 36, 82$ respectively. We have considered 4 different values of stratification with Brunt-Väisälä frequencies corresponding to Froude numbers $Fr = 0.8, 0.6, 0.16, 0.08$ and buoyancy Reynolds numbers Re_b in the range 0.2–35. We remark that for this flow the energy is composed by a kinetic and a potential contributions and, therefore, the viscous energy dissipation rate is typically smaller than the energy input rate ε since a fraction of the kinetic energy is converted into potential energy and removed from the system through the cascade of potential energy [14]. As a consequence, small-scale parameters η and τ_η have a small dependence upon stratification.

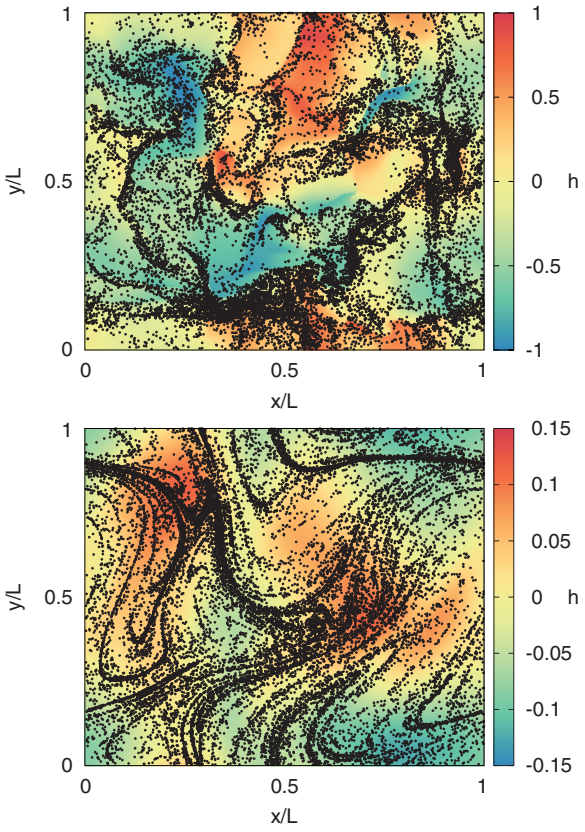

Fig. 1: (Color online) Snapshots of the distribution of inertial floaters with $St = 2$ over the isopycnal height h, implicitly defined by the equation $z - \theta = 0$ for simulations with $Fr = 0.4$ (top panel) and $Fr = 0.08$ (bottom panel). Resolution $M = 256$.

Once the turbulent flow has reached a statistical steady state, we introduce 20 populations of $M_p = 1.6 \times 10^5$ inertial tracers each, characterized by different St numbers between $St = 0.01$ and $St = 100$. The initial distribution for each population is uniform in the domain and their trajectories are evolved according to eqs. (3)–(5).

Figure 1 plots two snapshots of the particle distribution (for $St = 2.0$) together with the isopycnal surface h, implicitly defined by the equation $z = \theta(\mathbf{x}, t)$ for two

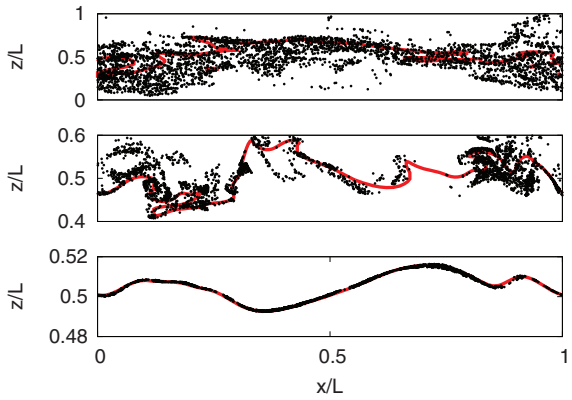

Fig. 2: (Color online) Snapshots of the vertical distribution of inertial floaters with $St = 2$ for increasing stratification strength (from top to bottom $Fr = 0.8, 0.4, 0.08$). Resolution $M = 256$.

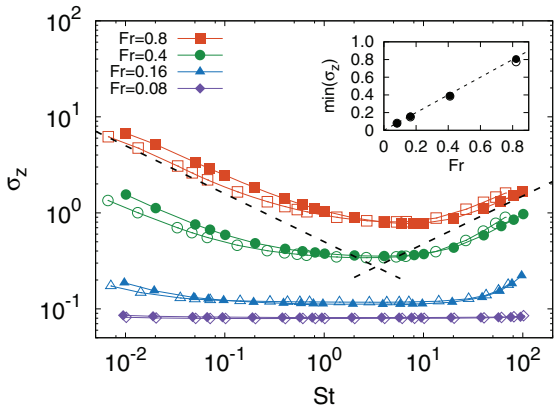

Fig. 3: (Color online) Layer thickness σ_z as a function of St for different stratification $Fr = 0.8$ (red squares), $Fr = 0.4$ (green circles), $Fr = 0.16$ (blue triangles), $Fr = 0.08$ (purple diamonds) and resolution $M = 128$ (empty symbols) and $M = 256$ (filled symbols). Dashed lines represent the behavior $St^{1/2}$ and $St^{-1/2}$. Inset: behavior of σ_z as a function of Fr in the case of maximum confinement.

values of stratification $Fr = 0.4$ (top panel) and $Fr = 0.08$ (bottom panel). We observe that the particles distribution is correlated with the interfacial regions between positive and negative values of θ. Such a correlation has been observed previously for inertial particles in homogeneous isotropic turbulence [15]. Indeed, once floaters have reached their isopycnal surface, they are constrained to perform a quasi-horizontal motion which is unaffected by gravity and resembles that of the inertial particles accumulating at the fronts.

The vertical distribution of particles is shown in fig. 2 for different values of stratification of the velocity field. The vertical confinement is produced by the last term in eq. (5) which is proportional to N^2, and it is therefore strongly dependent on stratification. For the most stratified case, $Fr = 0.08$, particles are practically confined on the isopycnal surface $z = \theta$, which correspond to the density $\rho = \rho_0$.

Statistics of vertical confinement. To better understand the mechanism of layer formation, we can first consider the limit of small St. For $\tau_p \to 0$, we can take the overdamped limit of eq. (5) which, after defining, $\tau = 3/(2N^2\tau_p)$, becomes

$$\dot{\mathbf{x}} = \mathbf{u} - \frac{1}{\tau}(z - \theta)\hat{\mathbf{z}}. \tag{6}$$

The comparison with eq. (2) shows that in this limit, neglecting diffusion, the quantity $(z - \theta)$ exponentially relaxes to zero with the characteristic time τ. Our numerical simulations confirm this picture, and the variance of the vertical position $\sigma_z^2 = \langle z^2 \rangle - \langle z \rangle^2$ (the brackets indicate a Lagrangian average) decreases from the initial value $\sigma_0^2 = \pi^2/3$ (corresponding to a uniform vertical distribution) and reaches a stationary value after a time of order τ. In the limit of small St, the particles distribution is almost homogeneous (with $\sigma_z = \sigma_0$), while for increasing St, σ_z drops down indicating that a layer of thickness smaller than the box length is formed.

The stationary root mean square of the vertical position as a function of the Stokes number and for different Froude numbers is shown in fig. 3 which confirms the qualitative observation of fig. 2: vertical confinement strongly depends on stratification, following the fluctuations of the isopycnal surface $z - \theta = 0$. For each Fr, we find a maximum confinement for intermediate values of the Stokes numbers, $St = O(1)$. This behavior can be understood since in the limit of small St the last term in eq. (6) is small (τ is large) and the particle trajectory is close to that of a fluid particle. In the opposite limit of large St, particles are unable to follow the rapid fluctuations of the isopycnal surface and this produces a thick layer around the isopycnal surface.

The above argument can be made more quantitative by considering the stochastic version of eq. (5) in which the fields $\mathbf{u}$ and θ are Gaussian noises with zero mean and variances $2D_u$ and $2D_\theta$. Formally, this is justified for $St \gg 1$, however, we will see that the model provides the correct scaling also for small St. The vertical motion of the floaters is therefore governed by an Ornstein-Uhlenbeck process for the probability $p(z, v)$ to find a particle at the vertical position z with a vertical velocity v. The associated Fokker-Planck equation is [16]

$$\partial_t p + \partial_z(vp) - \partial_v \left[\left(\frac{v}{\tau_p} - \frac{2N^2}{3} z \right) p \right] = D \partial_v^2 p \tag{7}$$

which has as solution a Gaussian distribution. The marginal distribution of particle positions is also Gaussian with variance $\sigma_z^2 = \frac{3\tau_p}{2N^2} D$, where

$$D = \frac{1}{\tau_p^2} D_w + \frac{4}{9} N^4 D_\theta \tag{8}$$

is the total diffusivity due to D_w, the eddy diffusivity due to the fluctuating turbulent velocity, and D_θ, the diffusivity due to the fluctuations of the stratification

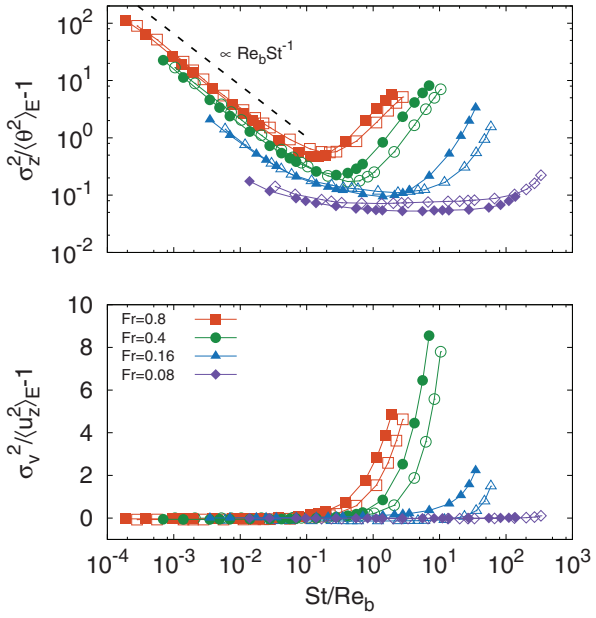

Fig. 4: (Color online) Variance of the layer thickness σ_z^2 normalized with the Eulerian-averaged variance of the fluctuation density field $\langle\theta^2\rangle$ (top panel) and variance of the vertical particle velocity σ_v^2 normalized with the Eulerian-averaged variance of the vertical fluid velocity $\langle u_z^2\rangle$ (bottom panel) as a function of St/Re_b for different stratification $Fr = 0.8$ (red squares), $Fr = 0.4$ (green circles), $Fr = 0.16$ (blue triangles), $Fr = 0.08$ (purple diamonds) and resolutions $M = 128$ (empty symbols) and $M = 256$ (filled symbols).

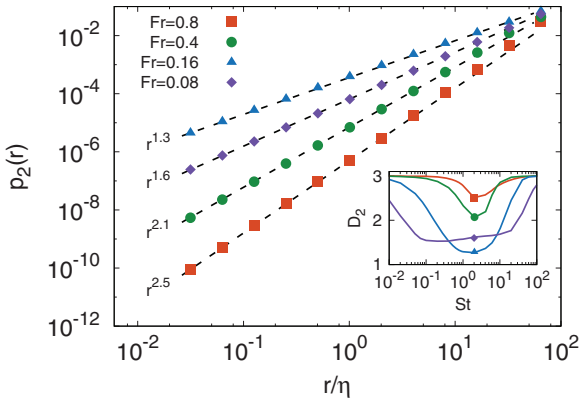

Fig. 5: (Color online) Correlation integral $p_2(r)$ as a function of r/η for different values of stratification $Fr = 0.8$ (red squares), $Fr = 0.4$ (green circles), $Fr = 0.16$ (blue triangles), $Fr = 0.08$ (purple diamonds) and Stokes number $St = 2$. Resolution $M = 256$. Inset: correlation dimension D_2 as a function of St for different stratification.

(we neglect the contribution in D due to the added mass since it does not change the following argument). The expression eq. (8) explains the non-monotonic behavior observed in fig. 3. Indeed for small τ_p the first term on the r.h.s. of eq. (8) dominates and we get the behavior $\sigma_z^2 \simeq 3D_w/(2N^2\tau_p) \propto Re_b St^{-1}$ (also observed in [17]), while in the opposite limit we get $\sigma_z^2 \simeq 2D_\theta N^2\tau_p/3 \propto Re_b^{-1} St$.

Figure 3 shows that σ_z strongly depends on the stratification, since for small Fr the isopycnal surface to which particles are attracted is more confined, as shown in fig. 2. This can be also understood from the stochastic model, eqs. (7), (8), in the limit of small St since there we have $\sigma_z \propto 1/N$ which is indeed close to the numerical results as shown in the inset of fig. 3 which confirms previous results obtained within the overdamped model [12]. We observe that in the opposite limit of large St, σ_z contains the diffusivity D_θ which is itself dependent on N.

In fig. 4, the variance σ_z^2 as a function of St/Re_b is shown for different stratifications. For small values St/Re_b, numerical results confirm the prediction of the stochastic model.

Statistics of vertical particle velocity. A similar argument using the Fokker-Planck equation (6) can be exploited to study the vertical particle velocity v. As before, the marginal distribution of particle velocity is Gaussian with variance given by $\sigma_v^2 = D_w\tau_p^{-1} + \frac{4}{9}N^4\tau_p D_\theta$. In fig. 4 (bottom panel), the vertical particle velocity v is observed to increase with St. In the limit of small inertia, the particle velocity has to coincide with the velocity of the surrounding fluid. In the opposite limit, when $St \gg 1$ the vertical particle velocity slightly differs from the fluid velocity and it is found to increase approximately as $St^{1/2}$. This is very different from the case of inertial particles, for which it has been observed that particle velocity decreases as $St^{-1/2}$ [18].

Small-scale fractal clustering. In addition to the vertical, large-scale inhomogeneity due to layering around the equilibrium isopycnal, particle dynamics induces small-scale clustering within the layer, which is evident from the horizontal section shown in fig. 1. This small-scale clustering is due to the dissipative dynamics, eq. (5), which governs the motion of the tracers and it is typical of inertial particles in incompressible turbulence. As a consequence, trajectories in phase-space converge onto a dynamic attractor of smaller dimension and, when the attractor has dimension smaller than the space dimension $d = 3$, particles distribute on a fractal set of the same dimension [5].

In order to characterize small-scale clustering we computed the correlation dimension D_2 of the particle distribution, defined through the probability $p_2(r) \sim r^{D_2}$ of finding two particles within a distance r. A homogeneous distribution in a d-dimensional space would clearly give $D_2 = d$. Figure 5 shows $p_2(r)$ for different values of St and Fr. A clear scaling range can be observed between 0.1η and 10η, from which one obtains a measure of the correlation dimension D_2. The correlation dimension as a function of St and for various values of Fr is plotted in the inset. In all cases, the strongest clustering is observed for intermediate values of St, while extreme (small or large) values of St produce more homogeneous layers. A similar phenomenology is also observed in the small-scale clustering of inertial particles also in homogeneous, isotropic turbulence [5].

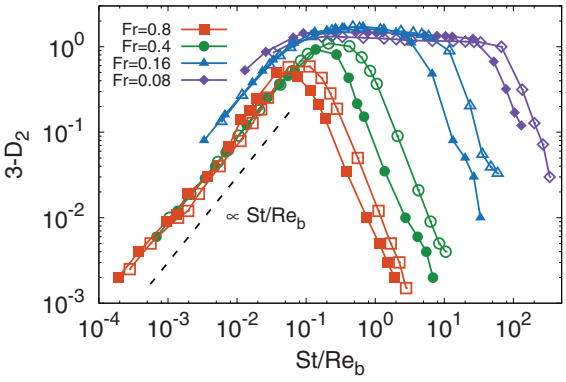

Fig. 6: (Color online) Co-dimension $3 - D2$ as a function of $Re_b^{-1}St$ for different stratification $Fr = 0.8$ (red squares), $Fr = 0.4$ (green circles), $Fr = 0.16$ (blue triangles), $Fr = 0.08$ (purple diamonds) and resolutions $M = 128$ (empty symbols) and $M = 256$ (filled symbols). Dashed line represents the prediction $Re_b^{-1}St$.

One can focus more precisely on the deviations from homogeneity (for which $D_2 = 3$) by considering the co-dimension $3 - D_2$, which is plotted in fig. 6 for the same values of Fr. This figure clearly shows a power-law increase of the co-dimension with St in the limit of low inertia.

However, comparison between fig. 6 and analogous measurements in the literature on inertial particles in isotropic turbulence show a striking difference in the small-St behavior of the curves. In the case where buoyancy is neglected one can show that $3 - D_2 \sim St^2$ for $St \to 0$ while in our case $3 - D_2 \sim St$ in the limit of small particles, as one can see in fig. 6. This behavior can be rationalized following [4,19,20]. In the small-St limit, one can again use the approximation of eq. (6), in which the particles are advected by an effective velocity field $\mathbf{v}(\mathbf{x}, t) = \mathbf{u} - (1/\tau)(z - \theta)\hat{\mathbf{z}}$. The number density of the particles evolves as $\mathrm{d}n/\mathrm{d}t = -(\nabla \cdot \mathbf{v})n = (1 - \partial_z\theta)/\tau$. The particle distribution will be homogeneous above a certain scale $\ell \gtrsim \eta$, with a constant number density n_0, and fractal on smaller scales due to the chaotic dynamics. If n is sampled with boxes of size $r \ll \ell$, the density fluctuations measured will be those accumulated along a Lagrangian trajectory during a time $T_r = \ln(\ell/r)/|\lambda_3|$, *i.e.*, the time it takes for chaotic advection to compress the initial patch along the direction characterized by the most negative Lyapunov exponent λ_3. One therefore has $n^2 \sim n_0^2 \exp[2\int_0^{T_r} \tau^{-1}(1 - \partial_z\theta)\mathrm{d}t]$. The Eulerian average requires to weigh each patch with its volume, which contracts as $1/n$ so one has

$$\langle n^2 \rangle = n_0^2 \left\langle \exp\left[\int_0^{T_r} \tau^{-1}(1 - \partial_z\theta)\mathrm{d}t\right]\right\rangle \sim \left(\frac{r}{\eta}\right)^{\alpha}. \quad (9)$$

If we assume the integral to be dominated by the constant term we get $\alpha = 1/(|\lambda_3|\tau)$. Of course this requires that $|\partial_z\theta| \ll 1$, *i.e.*, that the density fluctuations are small. This condition is typical for $Re_b \lesssim 1$: in this case, correlations of particle distributions with the gradients of θ do not compromise the validity of the argument. For small St it is reasonable to assume that $\lambda_3 \propto \tau_\eta^{-1} + O(1/\tau)$, so given the definition of the correlation dimension, $3 - D_2 = \alpha \simeq \tau_\eta/\tau \simeq Re_b^{-1}St$. Figure 6 shows that the prediction holds even at relatively large values of Fr and consequently Re_b. In this situation, the condition of small $\partial_z\theta$ is frequently violated, leading to several folds in the isopycnal. However, at moderate Re_b, folds will cover a rather limited area, so that for weak clustering (at small St) their contribution is probably still subleading. It may be interesting to notice that the behavior of D_2 is similar to that of $\langle\sigma_z\rangle$ in fig. 4. In particular, both observables have a minimum near $St \sim O(1)$. Moreover, both quantities shows a plateau in the region of maximum clustering, which becomes more evident when the fluid is intensely stratified.

Indeed, if Re_b is very small, isopycnals are very close to flat surfaces and vertical fluctuations are suppressed.

Conclusions. – We investigated the behavior of inertial particles advected by stratified turbulence, in the case of particle density intermediate within the fluid density gradient. We have studied how the interplay of gravity and turbulence produces a vertical confinement of the inertial particles around the isopycnal surface at the particle density, and how the resulting dissipative dynamics produces fractal clustering at small scales.

The interaction between particle settling and turbulence is an essential problem for many systems in the natural sciences and in applications. In marine and lake biology, the possibility of organisms to control their position in the water column is of great importance for the uptake of nutrients, the access to light and for escaping predators [21,22]. In the absence of specific mechanisms, the survival of such organisms must result from the complex interplay between turbulent mixing and growth [23,24]. A particularly interesting problem is posed by thin phytoplankton layers (TPL), aggregations of phytoplankton and zooplankton at high concentration, with thickness from centimeters to few meters, extending up to several kilometers horizontally and with a time scale from hours to days [2]. Various mechanisms have been proposed to explain such formations, notably depending on the motility (or absence thereof) of a particular species observed to form TPLs. In particular, If a cell is neutrally buoyant at some intermediate depth in the pycnocline, then buoyancy could lead to the formation TPLs [2,12,25].

The physical and biological implications of fractal clustering observed at small scales are associated with an increased probability to find particles at small separations with respect to a homogeneous distribution. Numerical studies inspired by TPLs showed that this can have important effects on the population dynamics of plankton [26]. In general, small-scale clustering is relevant in problems where encounter rates are

important, such as mating and competition for resources in biology, coalescence and coagulation of droplets in cloud physics [19,27] and engineering applications [28].

* * *

We thank M. Cencini for useful discussions. We acknowledge support from the COST Action MP1305 "Flowing Matter" and from Cineca within the INFN-Cineca agreement INF17turb.

REFERENCES

[1] Grabowski W. and Wang L.-P., *Annu. Rev. Fluid Mech.*, **45** (2013) 293.
[2] Durham W. and Stocker R., *Annu. Rev. Mar. Sci.*, **4** (2012) 177.
[3] Squires K. and Eaton J., *Phys. Fluids A: Fluid Dyn.*, **3** (1991) 1169.
[4] Balkovsky E., Falkovich G. and Fouxon A., *Phys. Rev. Lett.*, **86** (2001) 2790.
[5] Bec J., *Phys. Fluids*, **15** (2003) L81.
[6] Bec J., Homann H. and Ray S., *Phys. Rev. Lett.*, **112** (2014) 184501.
[7] Gustavsson K., Vajedi S. and Mehlig B., *Phys. Rev. Lett.*, **112** (2014) 214501.
[8] Riley J. and Lelong M.-P., *Annu. Rev. Fluid Mech.*, **32** (2000) 613.
[9] Bretthouwer G., Billant P., Lindborg E. and Chomaz J.-M., *J. Fluid Mech.*, **585** (2007) 343.
[10] van Aartrijk M. and Clercx H., *Phys. Rev. Lett.*, **100** (2008) 254501.
[11] van Aartrijk M. and Clercx H., *Phys. Fluids*, **22** (2010) 013301.
[12] Sozza A., De Lillo F., Musacchio S. and Boffetta G., *Phys. Rev. Fluids*, **1** (2016) 052401.
[13] Maxey M. and Riley J., *Phys. Fluids*, **26** (1983) 883.
[14] Sozza A., Boffetta G., Muratore-Ginanneschi P. and Musacchio S., *Phys. Fluids*, **27** (2015) 035112.
[15] Bec J., Homann H. and Krstulovic G., *Phys. Rev. Lett.*, **112** (2014) 234503.
[16] Gardiner C., *Stochastic Methods*, *Springer Series in Synergetics* (Springer) 1985.
[17] Birch D. A., Young W. and Franks P., *Limnol. Oceanogr*, **54** (2009) 397.
[18] Abrahamson J., *Chem. Eng. Sci.*, **30** (1975) 1371.
[19] Falkovich G., Fouxon A. and Stepanov M., *Nature*, **419** (2002) 151.
[20] Fouxon I., *Phys. Rev. Lett.*, **108** (2012) 134502.
[21] Reynolds C., *The Ecology of Phytoplankton* (Cambridge University Press) 2006.
[22] Kiørboe T., *A Mechanistic Approach to Plankton Ecology* (Princeton University Press) 2008.
[23] Huisman J., Arrayás M., Ebert U. and Sommeijer B., *Am. Nat.*, **159** (2002) 245.
[24] Margalef R., *Oceanol. Acta*, **1** (1978) 493.
[25] Alldredge A., Cowles T., MacIntyre S., Rines J., Donaghay P., Greenlaw C., Holliday D., Margaret M., Dekshenieks J. and Zaneveld J., *Mar. Ecol. Prog. Ser.*, **233** (2002) 1.
[26] Perlekar P., Benzi R., Nelson D. R. and Toschi F., *Phys. Rev. Lett.*, **105** (2010) 144501.
[27] Shaw R. A., *Annu. Rev. Fluid Mech.*, **35** (2003) 183.
[28] Post S. L. and Abraham J., *Int. J. Multiphase Flow*, **28** (2002) 997.